http://dx.doi.org/10.14500/aro.12333

Dolomitization and Hypogenic Dissolution of the Eocene Avanah Formation, Iraqi Kurdistan

Gazang H. Qadir[1†] and Howri Mansurbeg[2,3]

[1]Department of Earth Sciences and Petroleum, College of Science, Salahaddin University-Erbil, Erbil, Kurdistan Region – F.R. Iraq

[2]General Directorate of Scientific Research Center, Salahaddin University-Erbil, Erbil, 44001, The Kurdistan Region – F.R. Iraq

[3]Department of Geology, Palacký University, 17. listopadu 12, Olomouc 77146, Czechia

***Abstract*—This study constrains the mechanism of extensive dolomitization and its impact on reservoir quality of the shallow-water marine ramp carbonates of the Avanah Formation (Eocene), Iraqi Kurdistan. The presence of shoal deposits, which semi-isolate a lagoon water body from the open marine, suggests that dolomitization was by seepage reflux of brines. Nevertheless, the absence of eogenetic gypsum/anhydrite in the dolostones succession indicates that the dolomitizing fluids were mesohaline/penesaline brines formed during cycles of relative sea level (RSL) fall. Dolomitization resulted in the formation of abundant intercrystalline and moldic/vuggy pores. Restriction of dolomitization and related reservoir quality improvement to the lower part of the formation is attributed to an overall 3rd order fall in the RSL. Conversely, the lack of dolomitization in the upper part of the formation is attributed to deposition during 3rd order marine transgression, which prevented severe restriction and evaporation of the inner ramp and, consequently, inhibited the development of dolomitizing brines. It is suggested that hypogenic dissolution (karstification) by upward flow of aggressive fluids along faults and fractures during the Zagros Orogeny caused dissolution and considerable porosity and permeability improvement of the dolostones. A greater extent of dolostones dissolution in the flanks, which was accompanied by calcite cementation, compared to the crest, reflects the role of oil emplacement in the retardation of diagenetic reactions.**

***Index Terms*—Avanah formation, Dolomitization, Dolostones, Hypogenic karstification, Mesohaline/penesaline brines, Reservoir quality, Seepage reflux.**

I. Introduction

Dolomitization of marine platform limestones is still one of the most enigmatic near-surface diagenetic processes (Machel and Mountjoy, 1986; Braithwaite, 1991; Machel, 2004). There are debates regarding several dolomitization-related topics, including:

1. The numerous dolomitization models suggested in the literature face the same problems regarding the thermodynamics and kinetics of the reaction, the origin of Mg-rich dolomitizing fluids and patterns of mass supply, and the lack of modern analogs (Warren, 2000). Despite the suggestion of several models, the evaporative (Rameil, 2008; Morad, et al., 2012) and hydrothermal dolomitization (Katz, et al., 2006; Merino and Canals, 2011; Mansurbeg, et al., 2016) models have gained increasing support. Recent insights into dolomitization of limestones have been obtained by linking the process to changes in the relative sea level (RSL) (Morad, et al., 2012; Jia, et al., 2023).
2. The origin of closely associated intra-formational limestones and dolostones. Suggested mechanisms for this association include: (i) selective dolomitization of the more permeable grain-supported than matrix-supported limestones by hydrothermal fluids (Martín-Martín, et al., 2015; Koeshidayatullah, et al., 2020; Mansurbeg, et al., 2024), and (ii) controls on the degree of restriction of inner platform and seepage reflux of dolomitizing brines by cycles of rise and fall in the RSL (Morad, et al., 2023).
3. The effect of dolomitization on reservoir-quality improvement (Morrow, 1982; Lucia and Major, 1994; Sun, 1995; Machel, 2004; Ehrenberg, et al., 2006). It has long been argued that dolomitization of limestones causes improvement of reservoir quality. Nevertheless, the degree of improvement depends: (i) on the extent of post-dolomitization cementation of the resulting pores by mostly dolomite (referred to as over-dolomitization), calcite, and gypsum/anhydrite (Leary and Vogt, 1986; Lucia, 2004; Jones and Xiao, 2005; Martín-Martín, et al., 2015), and (ii) depositional texture of the precursor limestones, with most improvement occurring in the more permeable, grain-supported than in matrix-supported limestones (Morad, et al., 2023). Little emphasis has been made on the dissolution of dolostones during burial diagenesis. Furthermore, Ehrenberg, Walderhaug and Bjørlykke (2012) excluded the possibility of the formation of secondary porosity in carbonate successions during burial diagenesis.

ARO-The Scientific Journal of Koya University
Vol. XIII, No. 2(2025), Article ID: ARO.12333. 13 pages
DOI: 10.14500/aro.12333
Received: 04 June 2025; Accepted: 14 September 2025
Regular research paper; Published: 01 October 2025
†Corresponding author's e-mail: gazang.qadir@su.edu.krd

This paper, which deals with dolomitization of the shallow-water marine Avanah Formation (Paleocene-Eocene) in Iraqi Kurdistan (Fig. 1a-d), with the objectives of: (i) determining the stratigraphic distribution and extent of dolomitization, (ii) evaluating its influence on reservoir-quality evolution across the anticline, and (iii) assessing spatial variations in reservoir quality between flanks (water zone) and core areas (oil zone).

II. Geological Sitting

The Khurmala oilfield is situated within the Low Folded Zone of the Zagros Foreland Basin, which represents the outermost and least deformed part of the Zagros orogenic belt (Fig. 1a and b). This structural domain is characterized by broad, relatively open anticlines and synclines, with compression primarily driven by the northeastward convergence of the Arabian and Eurasian plates (Berberian,

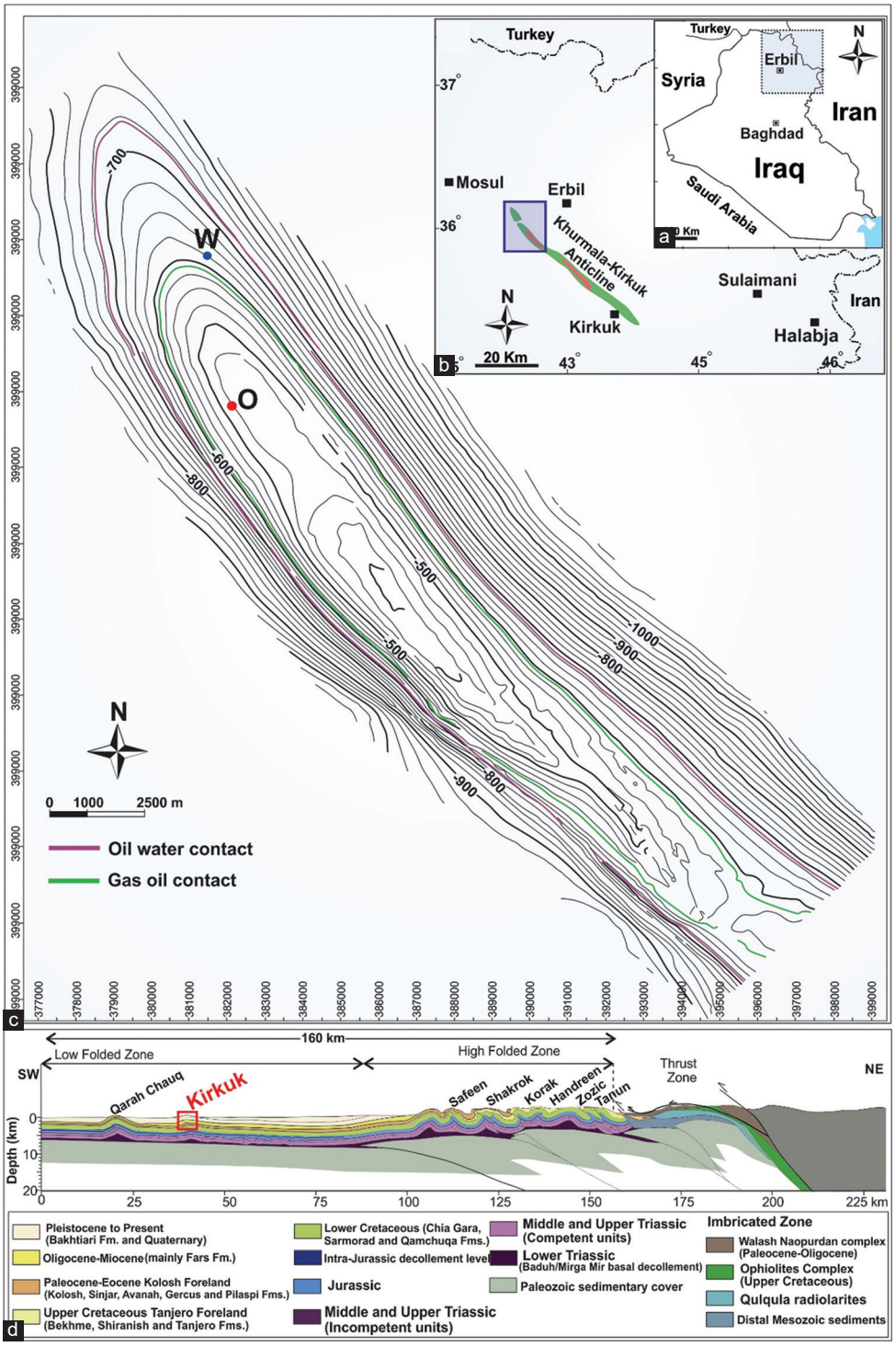

Fig. 1. (a and b) location of the studied Oil Field, Northern Iraq. (c) A structural contour map highlights the field's NW-SE orientation, well location, and key fluid contacts (gas-oil and oil-water) (Modified after Mahmood, et al., 2023). (d) A SW–NE geological cross-section illustrates major stratigraphy and structural zones controlling hydrocarbon accumulation (Modified after Le Garzic, et al., 2019).

1995; Alavi, 2004). The regional stratigraphy thickens towards the northeast, reflecting increasing subsidence and accommodation space along the foreland basin margin Sharland, et al., 2004; Jassim and Goff, 2006).

The Middle-Late Eocene Avanah Formation (50–250 m thick), which is a member of the Pila Spi Group within the Jaddala Megasequence, unconformably overlies the Khurmala Formation (Paleocene) is primarily composed of limestones, dolomitic limestones, and dolostones, representing lagoonal, near-shoal, and shoal facies characteristic of a shallow marine carbonate platform (Jassim and Goff, 2006; Aqrawi, et al., 2010; Fig. 2). Locally, the Avanah Formation inter-fingers with lagoonal dolomitized limestones of the coeval Pila Spi Formation (Khanaqa, 2011; Sissakian and Al-Jiburi, 2014).

At the type section in well Kirkuk-116, the formation comprises massive to bedded limestones (Avanah Dense), with notable dolomitization in the lower part (Avanah Porous). The less-altered Avanah Dense maintains primary depositional fabrics and contains abundant larger foraminifera, such as Nummulites and Discocyclina, suggesting a high-energy carbonate platform (Simmons, et al., 2007). The top of the Avanah Dense marks a regional sequence boundary, reflecting a period of subaerial exposure, erosion, and karstification, forming an unconformable contact with overlying units (Aqrawi, et al., 2010).

The Avanah Formation developed as part of a Middle Eocene rimmed carbonate platform associated with the Paleogene foreland basin. NW-SE trending shoals and reefal build-ups delineated this platform, separating the open marine Jaddala Basin to the southwest from the restricted lagoonal Pila Spi environment to the northeast (Aqrawi, et al., 2010). The lateral transition between the Avanah and Pila Spi formations is gradual, with interfingering facies, while the boundary with the Jaddala Formation is more abrupt, indicating a paleo-shelf margin (Jassim and Goff, 2006).

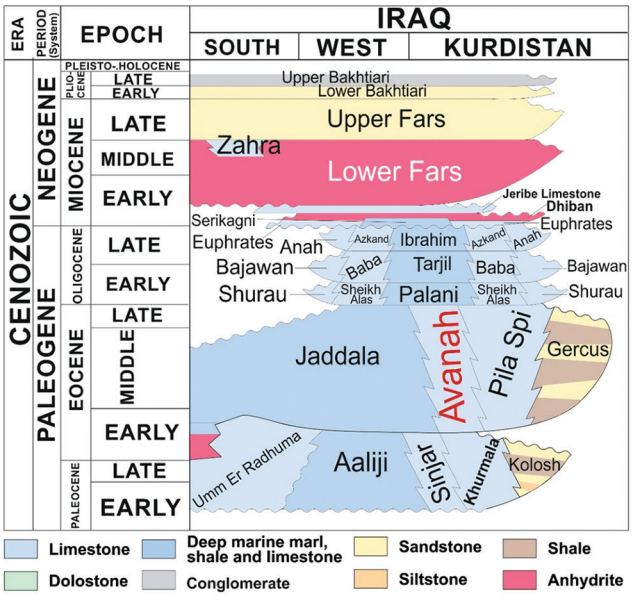

Fig. 2. Simplified stratigraphic column of Iraq, showing major formations and lithologies across the South, West, and Kurdistan regions from the Triassic to the Quaternary (Modified after Mansurbeg, et al., 2016).

The Avanah Formation serves as an important reservoir unit in three main oil fields of the Kirkuk region, specifically in the Avanah, Baba, and Khurmala domes of the Kirkuk anticline (Fig. 1a-c). Its hydrocarbon potential is linked to: (1) primary intergranular and moldic porosity, preserved in less dolomitized intervals, (2) fracture-enhanced porosity, particularly along anticlinal structures, (3) shoal and reefal facies, which provide localized reservoir sweet spots due to high primary porosity, and (4) diagenetic modification, which in some areas has improved permeability, while in others, excessive dolomitization and carbonate cementation have reduced reservoir quality (Ameen, 2009; Al-Ameri, 2010). Sealing potential is provided by overlying Oligocene shales or by tight intraformational carbonates. The primary hydrocarbon trapping mechanism is structural, with oil accumulation controlled by faulted anticlines (Ameen, 2009; Al-Ameri, 2010).

III. Samples and Analytical Methods

This study utilizes core material from two wells: One situated at the crest of the anticline (oil zone) and the other in the flank (water zone) of the field's anticline (Fig. 1c). All samples analyzed in this study are derived exclusively from these cores. Graphic logs were prepared for these wells based on careful examination of the texture, bioturbation, and sedimentary structures of the cored intervals (total of 19 m). Seventy core samples were selected from both the crest and flank of the anticline to constrain the impact of oil emplacement and diagenesis of the carbonate rocks of the Avanah Formation.

Thin sections were prepared for all the samples after being cleaned by Soxhlet extraction in toluene, dried, and vacuum impregnated with blue-colored epoxy to observe easier the pores under a conventional petrographic microscope. The thin sections were stained with alizarine red to readily distinguish between calcite and dolomite. Small chips from representative samples were analyzed using scanning electron microscopy (SEM) equipped with an energy-dispersive X-ray analyzer after coating with a thin layer of gold at the Department of Earth Sciences, Khalifa University, Abu Dhabi, United Arab Emirates. X-ray diffraction analyses of representative untreated bulk samples were performed to identify minor components such as clay minerals.

Porosity and permeability measurements were conducted on cleaned and dried cylindrical plug samples extracted from both horizontal and vertical orientations of the core material. The samples were subjected to standard cleaning using hot refluxing toluene to remove hydrocarbons and methanol to eliminate soluble salts, followed by drying at 116°C to a constant weight. Porosity was determined using the CMS-300™ Core Measurement System by applying Boyle's Law to helium expansion data, which was cross-validated with grain volume measurements obtained from the Ultra-pore™ 400 helium pycnometer. Porosity was calculated at both ambient and net confining stress conditions to capture the influence of overburden pressure on pore volume.

Permeability measurements were obtained using the same CMS-300™ system, employing a transient pressure decay method with helium gas to derive Klinkenberg permeability and equivalent air permeability. The system allowed automatic testing at multiple confining pressures ranging from 800 to 10,000 psig. For slabbed core sections, mini-permeability values were also measured using the Pressure Decay Profile Permeameter™, providing high-resolution vertical and lateral permeability profiles at specified intervals (40 points/m). These detailed datasets ensured accurate characterization of reservoir quality and heterogeneity across the analyzed intervals. Samples with permeability below 0.01 mD were excluded from statistical calculations to maintain data reliability. The core plugs used were one inch in diameter and two inches long.

IV. Results

A. Petrographic of Dolostones

The dolomitization occurs at depth intervals between ×61 m and ×73 m in the crest well and between ×016.62 m and ×077.70 m in the flank well, unconformably overlying the Khurmala Formation (Paleocene) (Fig. 3). Dolomitization has caused severe obliteration of the depositional texture of the precursor limestones. Nevertheless, the limestone textures can be inferred from the following observations: (i) the moldic pores are dissolved allochems, and (ii) the surrounding dense fine-crystalline dolomite represents dolomitized depositional matrix, whereas the rhombic dolomite crystals (40–85 μm) with intercrystalline pores are intergranular depositional pores. Further verification of the depositional texture of the precursor limestones is obtained by comparing the dolostone textures with those of undolomitized limestones, which dominate in the upper part of the Avanah Formation (Fig. 3).

However, the rounded grains, which are composed of dense microcrystalline (<4 μm) dolomite (Fig. 4a) with a similar size to the moldic pores are considered to be dolomitized peloids (Fig. 4a). In some cases, these microcrystalline dolomite grains have the shapes of bivalve fragments (Fig. 4b). Other skeletal fragments that are still recognizable include miliolids, textularids, alveolinids, bivalves, gastropods, and echinoderms (Fig. 4c). Using these criteria, the limestone precursors include mainly wackestones, packstones and grainstones, which on complete dolomitization are referred

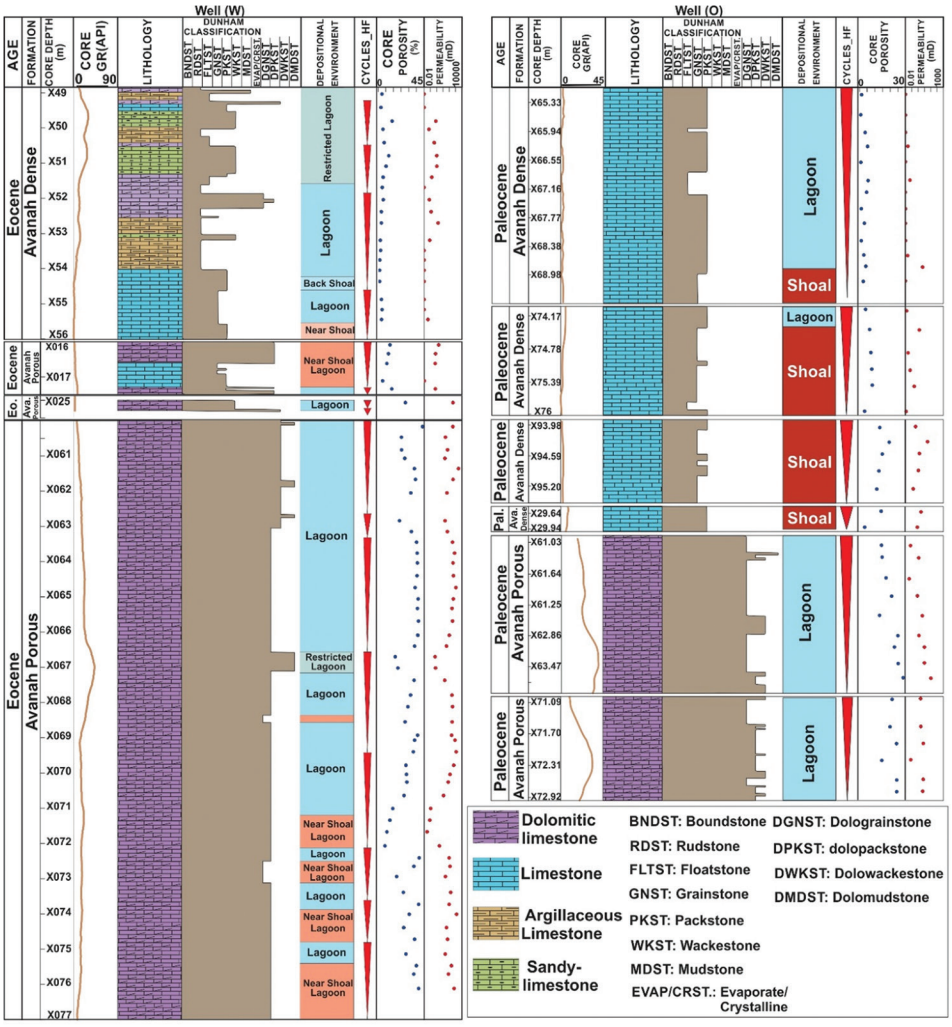

Fig. 3. Stratigraphic correlation between flank (Well W) and crest (Well O) wells in the Avanah Formation, showing lithology, facies, and depositional environments. Crest intervals are dominated by shoal facies, while the flank is mostly lagoonal.

http://dx.doi.org/10.14500/aro.12333

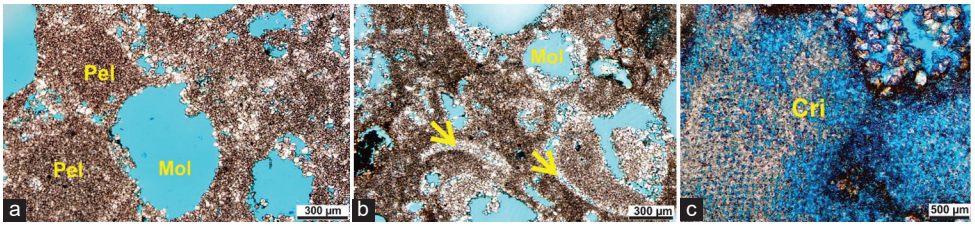

Fig. 4. Optical photomicrographs showing: (a) dolomitized peloids (Pel), (b) dolomitized microporous micritized bivalves (arrows), and (c) dolomitized and substantially dissolved crinoid fragments (Cri).

to as dolowackestones, dolopackstones, and dolograinstones, respectively.

The moldic pores and vugs are commonly empty or only lined by fine-crystalline dolomite (<20 µm across) with scalenohedral and, less commonly, rhombic crystal shapes (Fig. 5a). Moldic pores that are extensively filled by rhombic dolomite cement (40–120 µm across) are relatively uncommon (Fig. 5a-e). These rhombic dolomite crystals display a thin layer of dolomite overgrowths (Fig. 5f). In some cases, such dolomite cement has similar crystal shapes as equant calcite cement (Fig. 5c).

Unlike the dense microcrystalline dolomite, rhombic dolomite cement commonly contains intragranular vug-like pores formed by dissolved crystal cores (Fig. 6a-d). These intragranular pores, which occur within the rhombic dolomite crystals, are frequently filled with bituminous/dead oil (Fig. 6a-c). SEM examinations revealed that the microcrystalline dolomite is also severely etched (Fig. 7a-c). The intercrystalline and intracrystalline pores in these rhombic dolomites are locally cemented by coarse-crystalline, poikilotopic calcite (Fig. 8a). This coarse blocky calcite cement, which occurs as macro- and micro-nodules (Fig. 8b), is encountered in dolopackstones and dolograinstones of the water zone (the flank well) while completely absent in the oil zone (the crest well). Microfracture-filling calcite cement is common in the calcite cemented dolostones (Fig. 8a and b). In some cases, the intercrystalline calcite cement extends from the calcite cemented microfractures (Fig. 9a and b). Locally, the rhombic dolomite crystals are covered by tiny K-feldspar crystals (around 10 µm across) (Fig. 7c).

Scattered vugs in the dolostones are filled with blocky calcite, which is rarely associated with blocky anhydrite cement and saddle dolomite (Fig. 9c). Neither the moldic pores nor the vugs display evidence of collapse. Instead, brittle deformation has caused fragmentation/brecciation of the blocky calcite and dolomite crystals (Fig. 9a-c). The porous dolowackestones and peloidal dolopackstones contain stylolites (sutured and rectangular) and dissolution seams, which are locally segmented or irregular in continuity and are marked by dark bituminous organic matter (Fig. 10c-f). Locally, microfractures, which are filled with calcite cement, are arranged at high angles to and, in some cases, cut across the dissolution seams/stylolites (Fig. 10e and f).

B. Depositional Model

The distribution of depositional textures (sensu Dunham, 1962), sedimentary structures (cross- and flaser-stratification),

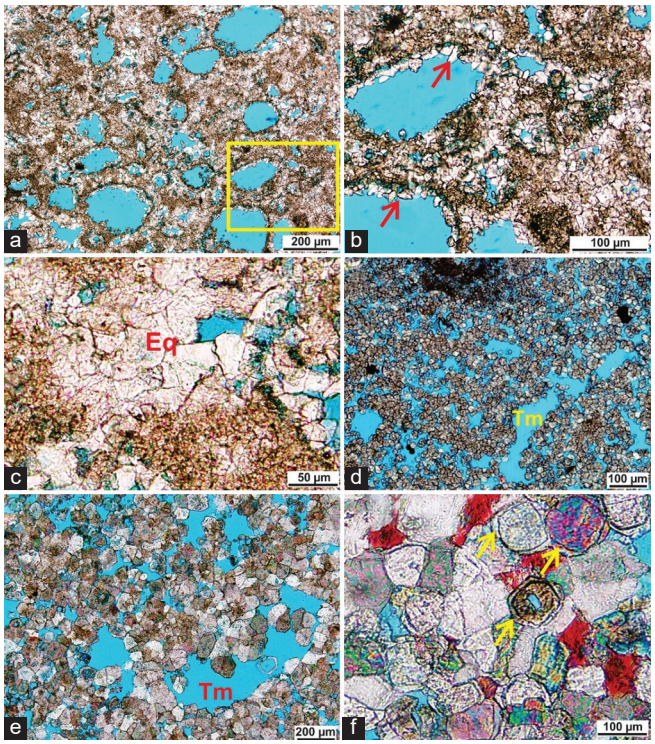

Fig. 5. Optical photomicrographs showing: (a) Dolopackstone with numerous scattered moldic pores (blue). (b) Higher magnification of the square in Figure A showing the presence of pore-lining scalenohedral (arrows), (c) Moldic pore in dolopackstone filled with equant dolomite (Eq), (d) Dolowackestone with touching moldic pores (Tm), (e) Dolograinstone in which the moldic pores are partially filled with dolomite cement. (f) Vug in dolograinstone with rhombic dolomite displays a thin layer of dolomite overgrowths (arrows).

the extent and type of bioturbation (Planolites and Thalassinoides), and the faunal assemblage (algae, corals, stromatoporoids, benthic foraminifera, bivalves, gastropods, and echinoderms) were analyzed. These features collectively indicate that deposition took place in a shallow-water, wave-tide-dominated marine homoclinal ramp setting (Fig. 11). This setting comprises an intertidal and subtidal (lagoon) environments, which are separated from the open marine by skeletal shoal deposits. The open marine environments include slope and basin floor environments. The limestone textures and their equivalent dolostones include dominantly: (i) wackestones and packstones, which were deposited in the intertidal-subtidal environments, (ii) grainstones, which were deposited in shoals, and (iii) mudstones deposited in offshore environments.

C. Porosity and Permeability of Dolostones

The dolostones contain variable proportions of intercrystalline, intracrystalline, and moldic/vuggy pores. The intercrystalline pores are most abundant between the rhombic dolomite crystals in the dolograinstones (Fig. 10f and e) and between dolomite rhombs filling the moldic pores and vugs (Fig. 10c). The intercrystalline pores are associated with pervasive dissolution of the intergranular and moldic pore/vug filling rhombic dolomite and, locally, cementation by poikilotopic calcite (Fig. 10a and b). The microcrystalline dolomite formed by dolomitization of mud matrix and peloids contains micropores <5 μm across and scattered microvugs (10–15 μm). The dolopackstones and dolograinstones contain variable amounts of moldic pores (around 100–1,500 μm), which are embedded in intergranular rhombic dolomite cement and/or microcrystalline dolomitized matrix (Fig. 6a and B). These moldic pores display various degrees of connectivity with or touching each other (sensu Lucia, 2004) and with the overall pore system, and consequently contributed differently to the permeability of the dolostones. The touching and expansion of the adjacent moldic pores resulted in the formation of vugs (Fig. 5d and e). The bivariate plot of porosity and permeability for the Avana poros, for both flank (W) and crest (O) wells, is shown in Fig. 12. The crest shows lower porosity (12.5–29%, average 20.5%) and permeability (0.10–81 mD, average 10 mD), while the flank exhibits a broader porosity range (6.5–40.1%, average 30%) and significantly higher permeability (0.10–1780 mD, average 262 mD).

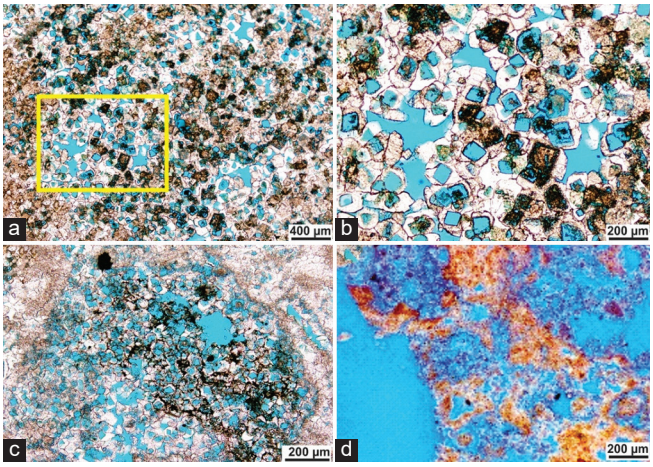

Fig. 6. Optical photomicrographs showing: (a) Dolograinstone in which a vug is filled with rhombic dolomite with dissolved cores, i.e., intracrystalline pores, (b) Higher magnification of the square in A showing that dolomite overgrowth is preserved, (c) Vug filled with dissolved rhombic dolomite and containing bitumen. (d) Severely dissolved dolostones in the flank well.

V. Discussion

The lithofacies distribution, petrophysical analyses, and petrographic characteristics of the Eocene carbonate succession provide important insights into the complex pattern of dolomitization and post-dolomitization processes in shallow-water ramp limestones and of their impact on the distribution of reservoir quality across the anticline.

A. Dolomitization Model: Relationship to Change in RSL

Deposition of the Eocene carbonates in a ramp setting with shoal deposits restricting the connectivity between the lagoon and open marine (Fig. 13) promotes dolomitization by seepage reflux of Mg-rich brines. These brines, which have a wide salinity range (72–520%), develop by evaporation of the lagoon water body during repeated episodes of significant fall in the RSL (Omidpour, et al., 2022). The lack of eogenetic gypsum/anhydrite indicates that the dolomitizing brines were undersaturated with respect to Ca-sulfates. These bines were thus mesohaline and not hypersaline in composition (Qing, Bosence and Rose, 2001; Rameil, 2005). Mesohaline and penesaline brines (salinities vary from 38% to 140%; Adams and Rhodes, 1960; Warren, 2000; Laya, et al., 2021) are saturated with respect to dolomite but undersaturated with respect to calcite, making them efficient dolomitization waters (Al-Helal, Whitaker and Xiao, 2012). The development of the mesohaline rather than hypersaline brines was presumably promoted by the warm subtropical paleoclimatic conditions during the middle Eocene (Al-Zubaidi and Al-Badrani, 2019).

The restriction of dolostones to the lower part of the formation suggests that carbonate deposition and dolomitization to 3rd order fall in RSL (Fig. 14). Repeated 4th and 5th order (minimum of 100 to 10 Ka, respectively; Figs. 13 and 14) cycles of RSL of carbonate deposition and dolomitization were imposed on 3rd order fall in RSL (duration 1–5 Ma). The 5th order changes in the RSL are

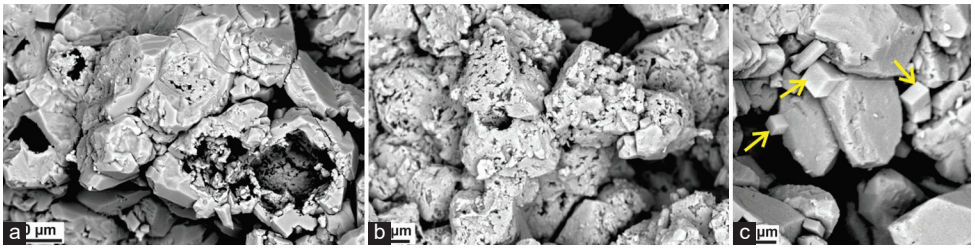

Fig. 7. Scanning electron microscopy (SEM) photomicrographs showing (a) dissolved cores of rhombic vug-filling dolomite, (b) partly dissolved micro-rhombic dolomite in dolowackstone. SEM image showing the presence of tiny K-feldspar crystals (arrows) commonly covering the dolomite crystals.

http://dx.doi.org/10.14500/aro.12333

commonly driven by Milankovitch/orbital forcing cycles (Kerans and Tinker, 1997). Brine pumping/reflux is expected to be most efficient at the end of the 4th and 5th cycles (i.e., along parasequence boundaries; Figs. 13 and 14) before the onset of the subsequent marine transgression.

The lack of dolomitization in the upper part of the formation suggests that deposition occurred during an episode of 3rd-order relative sea-level rise (Fig. 14). In the latter case, the episodes of fall in the 4th and 5th orders fall in RSL were not significant enough to cause restriction of the inner ramp and development of dolomitizing brines. The dolomitizing brines could have been provided by seepage reflux, tidal pumping, and evaporative pumping (Carballo, Land and Miser, 1987; Mazzullo, 2000; Jones and Xiao, 2005; Fig. 13). Thus, the development of such brines is attributed to combined effect of high-frequency fall in the RSL and semi-arid paleoclimatic conditions in the basin during the Eocene, which caused evaporation of surface and pore waters in the inner platform (Figs. 13 and 14).

Dolomitization involves the dissolution of $CaCO_3$ (aragonite and calcite) and the reprecipitation of dolomite. The formation of substantial volumes of moldic porosity suggests that the rate of dissolution of the metastable aragonitic allochems exceeded the rate of dolomite precipitation (Morad, et al., 2023). The limited porosity enhancement on dolomitization of lime mudstones and wackestones is attributed to their low depositional permeability, which caused low flow rates of dolomitizing fluids and removal of dissolved $CaCO_3$. These conditions result in more equal-volume dolomitization, i.e., creation of limited intercrystalline pores. Likewise, the replacement of peloids and severely micritized allochems by microcrystalline dolomite (Fig. 4a and b) resulted in the formation of abundant intercrystalline microporosity. Conversely, the high depositional permeability of packstones and grainstones induces higher rates of calcite/aragonite dissolution than the rate of dolomite precipitation, resulting in coarse-crystalline dolostones containing more intercrystalline (cf. Wierzbicki, et al., 2006; Roberts, et al., 2013; Morad, et al., 2023). Coarse-crystalline dolostones may also form brines with low concentrations of Mg^{2+} (cf. Wahlman, 2010). Thus, in addition to the impact of porosity, permeability, and reaction kinetics, dolostone texture is also controlled by the degree of saturation of the brines with respect to dolomite.

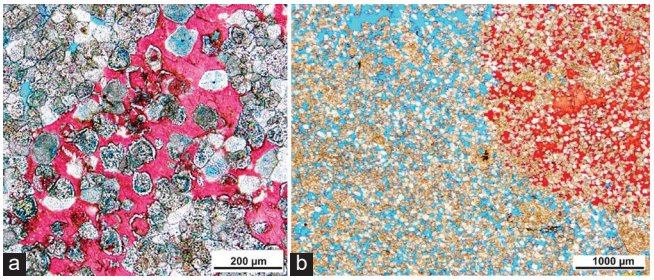

Fig. 8. Optical photomicrograph showing: (a) intercrystalline calcite cement (stained red) between rhombic dolomite crystals in dolograinstone; note that the dolomite crystals display various degrees of dissolution. (b) calcite-cemented patches in dolostones occur as rounded micronodules.

B. Dissolution of the Dolostones and Dolomite Cement

Dissolution of the dolostones across the anticline and concomitant precipitation of fracture-filling and intercrystalline calcite cement in the flanks are attributed to the flow of aggressive/unsaturated fluids (Fig. 15). These fluids are commonly characterized by elevated concentrations of water-soluble organic acids, carboxylic acid, CO_2 and sulfuric acids, which is referred to as hypogenic karstification (Klimchouk, 2000; Figs. 15 and 16). Organic acids, also called short-chain aliphatic acids or volatile fatty acids (e.g., acetate, oxalic, formate, and butyric acids) were suggested to be responsible for mineral dissolution and creation of secondary porosity (Surdam, Boese and Crossey, 1984; Lundegard and Land, 1986; MacGowan and Surdam, 1990; Crossey, et al., 1991; Fig. 16). The processes suggested for the formation of these acids include thermocatalytic degradation of kerogen in source rocks (Carothers and Kharaka, 1978), interaction between crude oil and water in petroleum reservoirs (Boles, 1992; Franks, et al., 2001), and hydrous pyrolysis of kerogen (Kawamura, et al., 1986; Eglinton, Curtis and Rowland, 1987; Barth, et al., 1991; Dias, 2000). The types and concentrations of organic acids derived on thermal maturation are controlled by the type of precursor organic matter (Li, et al., 2021).

The organic acids, which diffuse rapidly out of the oil phase and dissolve in the surrounding water phase (Palmer and Drummond, 1986; Barth, 1991), can cause substantial dissolution of carbonate reservoirs (Chen, et al., 2022;

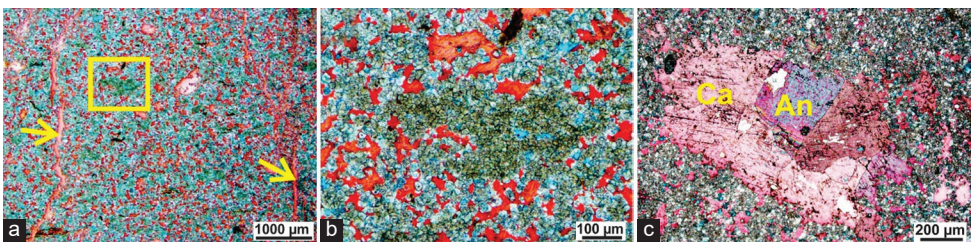

Fig. 9. Optical photomicrographs showing: (a) large patches of intercrystalline calcite cement (stained red) occur in the vicinity of calcite-cemented microfractures (arrows), (b) higher magnification of the square in A showing that the intercrystalline calcite cement has partly replaced the dolomite. (c) a vug in microfractured dolowackstone filled with coarse calcite (Ca) and anhydrite (An) crystals.

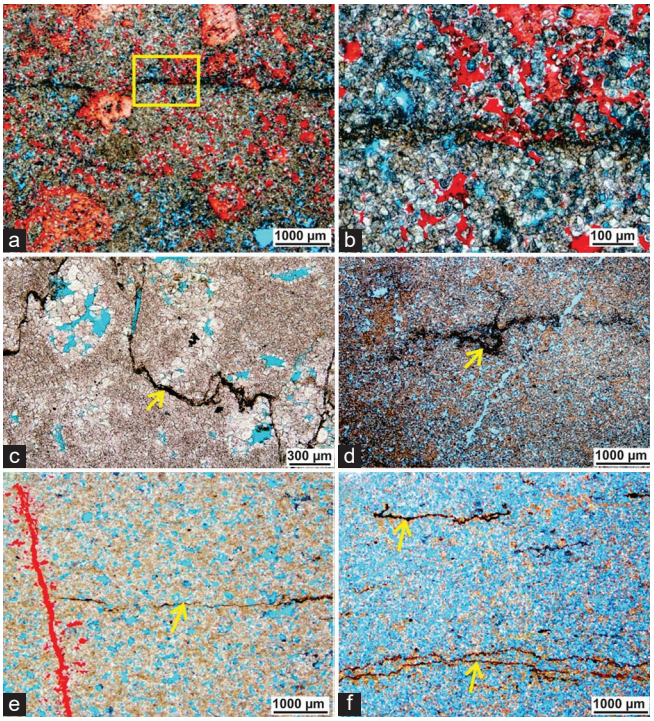

Fig. 10. Optical photomicrographs showing: (a) Dissolution seam around which the dolowackstone in cemented by calcite (stained red). (b) Higher magnification of the square in A. (c) Stylolite (arrow) in pleoidal dolopackstone along which the adjacent moldic pores are cemented by equant and rhombic dolomite. (d) Local dissolution seam (arrow) dolomudstone cut by empty microfracture (tension gash; arrow). (e) Local dissolution seam (arrow) in dolowackstone cut by tension gash filled with calcite cement (stained red). (f) Severely dissolved dolowackstone containing two discontinuous dissolution seams (arrows).

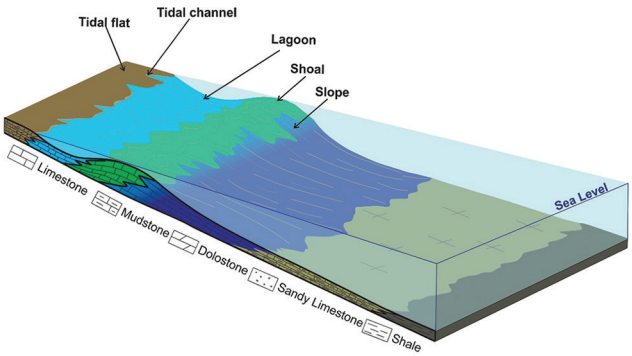

Fig. 11. The simplified conceptual model for Avanah Formation shows the transition from tidal flats to slope across a carbonate ramp, illustrating key environments: tidal channel, lagoon, shoal, and slope.

Fig. 16). Formation of carboxylic acids in sedimentary basins has been attributed to cleavage of kerogen containing carboxylate functional groups during the early stages of thermal maturation (Lundegard, Land and Galloway, 1984; Surdam, Boese and Crossey 1984; Cooles, Mackenzie and Parkes, 1987; Giles and Marshall, 1986). Potential sources of CO_2 include thermal decarboxylation of short-chain aliphatic acid anions (principally acetate) (Carothers and Kharaka, 1980). Hence, migration of the dissolved organic

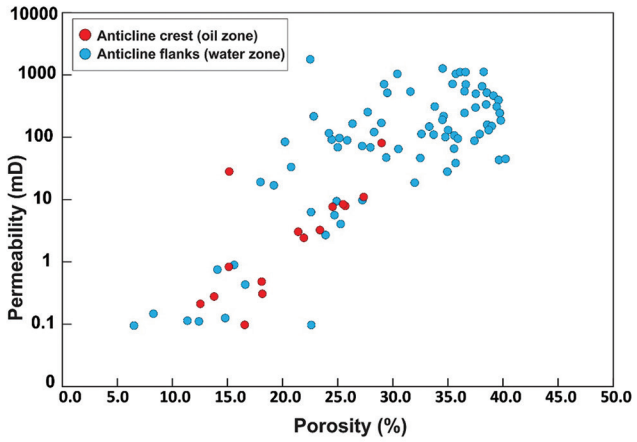

Fig. 12. Cross plot of permeability versus porosity of the dolostone core samples of the Avanah Formation from the flanks have greater values in the flanks (water zone) compared to the crest (oil zone) of the field's anticline.

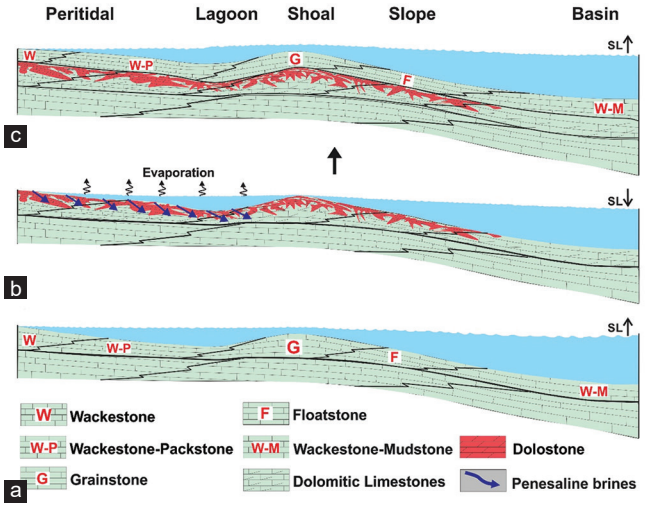

Fig. 13. Conceptual model illustrating dolomitization of the Avanah Formation carbonate platform during sea-level fall, driven by seepage-reflux processes. Penesaline brines generated in restricted lagoonal settings migrate basinward, progressively replacing original carbonate facies (wackestone, packstone, grainstone, floatstone, and mudstone) with dolostone across the lagoon, shoal, and slope environments.

and carboxylic acids is faster than that of oil and can potentially cause the creation of secondary porosity before oil emplacement in dolostones of the Avanah Porous reservoir (Fig. 16).

Sulfuric acid is formed by oxidation of H_2S formed by thermochemical sulfate reduction (TSR) upon upward migration into oxygenated waters (Jones, et al., 2003; Palmer, 2013). The relatively shallow burial depths of the Avanah Formation may allow the percolation of meteoric waters being facilitated by the presence of hydraulic head formed by tectonic uplift due to the Zagros Orogeny (Tavakoli and Barfizadeh, 2024; Fig. 15). TSR, which takes place at temperatures >130°C (Morad, et al., 2019), is expected to occur in the anhydrite-bearing, Upper Triassic Kurra Chine

http://dx.doi.org/10.14500/aro.12333

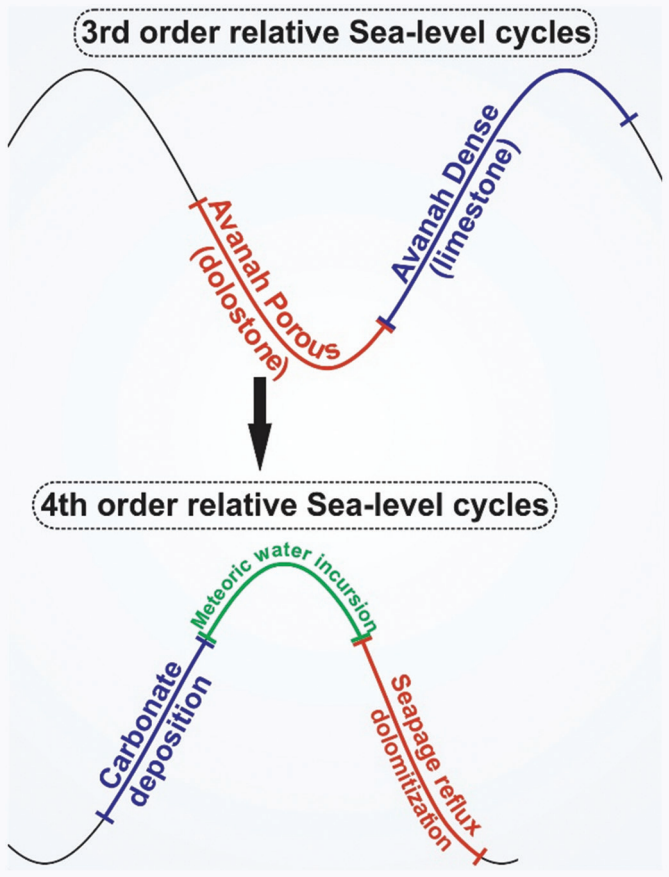

Fig. 14. Model showing how 3rd- and 4th-order relative sea-level cycles control the formation of Avanah porous (dolostone) and Avanah dense (limestone), with 4th-order cycles influencing meteoric water incursion, carbonate deposition, and seepage reflux dolomitization.

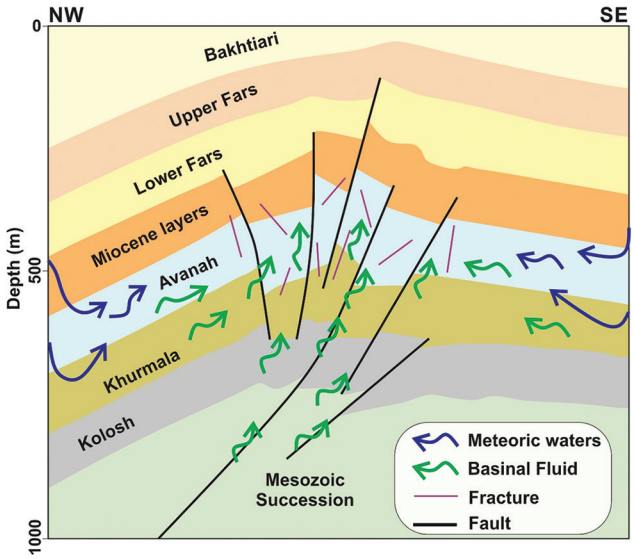

Fig. 15. Conceptual model showing meteoric and basinal fluid migration through faults and fractures, highlighting their role in fluid flow and diagenesis within the Avanah Formations.

Formation within the basin (Fig. 15). Laboratory experiments have demonstrated that sulfuric acid can cause substantial dissolution of dolomite (Joseph, et al., 2022). It has been

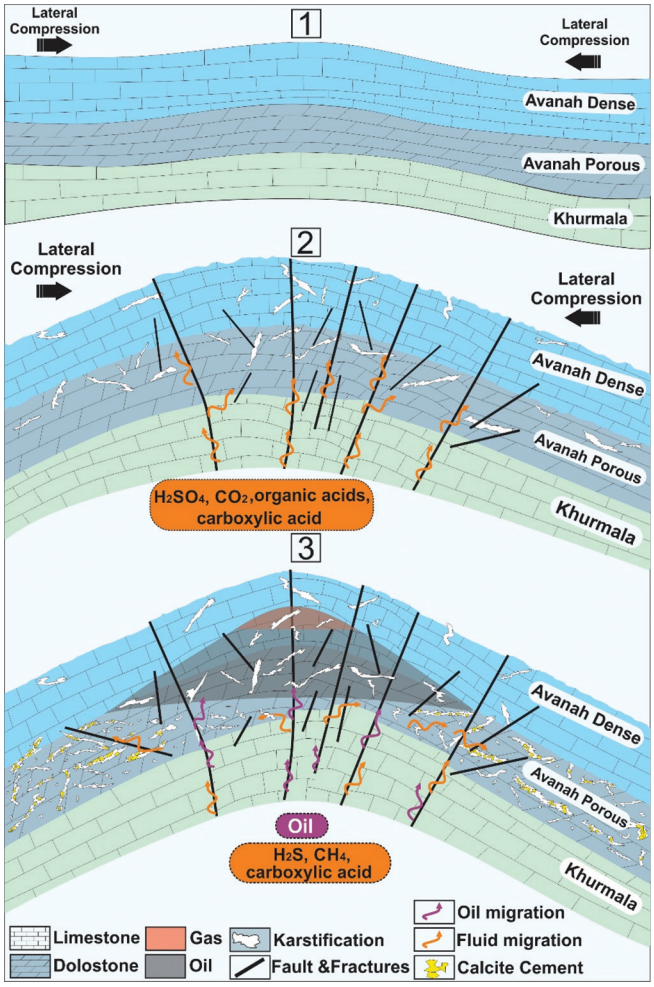

Fig. 16. Conceptual model illustrating the effects of lateral compression on the Avanah anticline. Faulting and fracturing promoted the upward migration of acidic basinal fluids enriched in CO_2, H_2SO_4, and organic acids, which induced hypogenic karstification and dolostone dissolution, enhancing porosity within the Avanah porous interval. Later oil emplacement inhibited further dissolution, triggered CO_2 degassing, and promoted localized calcite cementation, particularly along the flanks of the structure.

argued that basinal acidic fluids charged with carboxylic and organic acids can migrate over great distances both vertically and laterally just ahead of migrating hydrocarbon (Hanor, 1994; Mazzullo, 2000; Chen, et al., 2022). This interpretation is supported by the presence of bitumen in intracrystalline pores within dissolved rhombic dolomite (Fig. 6a-c).

The greater extent of dissolution and resulting improvement in reservoir quality in the flank compared to the crest dolostones of the Avanah anticline is evident from the porosity-permeability trends in Fig. 12. This difference is interpreted to reflect the role of oil emplacement in retarding diagenetic alteration, as minerals have negligible solubility in oil (e.g., Cox, et al., 2010). The impact of oil emplacement on the diagenetic evolution of the dolostones is further manifested by the restriction of calcite cementation to dolostones in the flank well (Fig. 16). The cementation event and replacement of dolomite by calcite indicate that the aggressive fluids ultimately became saturated with respect

to calcite probably as a consequence of CO_2 degassing subsequent to oil emplacement (Cosmo, et al., 2023). The common spatial connectivity of calcite cementation of the intercrystalline pores in dolostones with micro-fracture-filling calcite (Fig. 10a) suggests that these fractures acted as conduits for fluid migration and degassing (Fig. 15).

The flow of basinal brines into the dolostones is supported by the presence of authigenic K-feldspar ($KAlSi_3O_8$) crystals covering the undissolved dolomite overgrowths and of vug-filling anhydrite cement (Figs. 7c and 9c; Hearn and Sutter, 1985; Spötl, et al., 1998). Moreover, the formation of K-feldspar requires the transport of Al^{3+}, which has extremely low solubility in most basinal fluids except those containing significant amounts of dissolved organic acids. These acids significantly increase the mobility of aluminum and transport it as an organic complex in aliphatic acid solutions (Surdam, Boese and Crossey, 1984).

The occurrence of both dissolutions of dolostones and cementation by calcite in the vicinity of seams/stylolites and fractures suggests that these acted both as conduits for the flow of acidic fluids and sites of CO_2 degassing, respectively. The latter process is commonly related to a decrease in reservoir pressure (Smith, Ditmire and Tisch, 1998; Turner and Collins, 2013), probably occurring preferentially in areas in which permeability conduits were created by dolostone dissolution (Klimchouk, 2017). It has been argued by several authors that fluid flow along seams/stylolite occurs during lateral tectonic compression of sedimentary basins (Paganoni, et al., 2016; Morad, et al., 2019). The presence of local calcite cementation indicates that CO_2 degassing occurred locally and/or due to lateral and vertical variation in pressure (Turner and Collins, 2013). Local cementation by calcite can also be attributed to oxidation of oil caused by incursion of meteoric waters (Schulz-Rojahn, Ryan-Grigor and Anderson, 1998).

C. Paragenetic Sequence of the Diagenetic and Reservoir-Quality Evolution Events

The diagenetic and reservoir-quality evolution of the Eocene carbonates was accomplished during eogenesis and mesogenesis (Snsu Choquette and Pray, 1970; Fig. 17). Before dolomitization, the carbonate sediments were subjected to minor eogenetic alterations, which had a limited impact on reservoir quality. These alterations include: (i) partial cementation by pore-lining scalenohedral calcite, which is typically attributed to marine pore waters, and (ii) partial dissolution of the allochems and concomitant cementation by equant intergranular and intragranular calcite by incursion of meteoric waters. Subsequently, the sediments were subjected to dolomitization of the allochems, mud matrix, and earlier-formed calcite cements. Eogenetic dolomitization by seepage reflux of mesohaline/penesaline lagoonal brine caused the formation of various amounts of moldic and intercrystalline pores, which were controlled mostly by the depositional texture of the precursor limestones. Seepage reflux dolomitization, which involves the dissolution of the precursor limestones, caused various degrees of improvement in porosity and permeability of the precursor limestones.

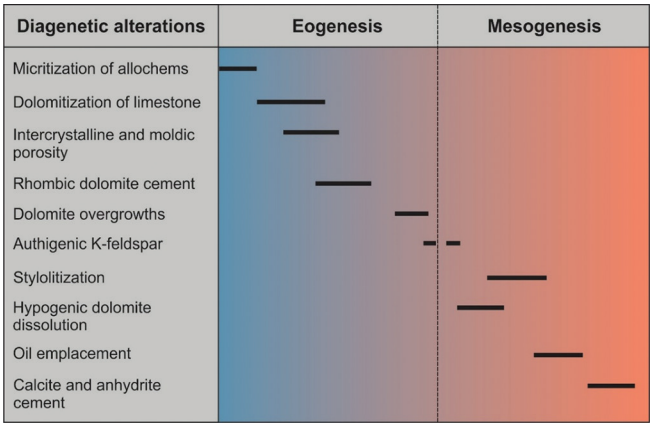

Fig. 17. Paragenetic sequence showing the relative timing and duration of the main diagenetic minerals/processes in the studied Avanah Formation.

The mesogenetic alterations include the development of dissolution seams and stylolites and the flux of acidic basinal fluids and deeply percolated meteoric waters, which caused substantial dissolution and improvement in the reservoir quality of the dolostones. The dissolution seams/stylolites acted, together with the faults and fractures, as conduits for the flow of acidic fluids, causing dolostones dissolution and the flow of calcite-saturated fluids that caused calcite cementation of the dolostones. This hypogenic dissolution event was later retarded/halted in the crest of the anticline due to the emplacement of hydrocarbon, while it continued in the flanks, being locally associated with cementation of the intercrystalline, intracrystalline, and moldic/vuggy pores by calcite, dolomite overgrowths, and trace amounts of K-feldspar and anhydrite. The retardation of flux of the acidic fluids in the crest of the anticline caused the poorer reservoir quality of the dolostones than those in the flanks (Fig. 12). Variations in the extent of porosity and permeability enhancement in the dolostones are attributed to depositional texture of the precursor dolostones as well as the degree of cementation of the flank dolostones by intercrystalline calcite. This situation of better reservoir quality in the flanks than in the crest carbonates is the opposite of the finding of other papers showing better reservoir quality in the crest than in the flanks carbonates (Heasley, Worden and Hendry, 2000; Paganoni et al., 2016; Morad, et al., 2018). In these cases, the poorer reservoir quality in the flanks is attributed to continued cementation in the water zone while retarded in the oil zone, leading to porosity preservation. The preservation of dolomite overgrowths has been attributed by Morad, et al. (2023) to greater crystal structural disorder than the dissolved cores. Consequently, the results and interpretation of hypogenic/mesogenetic dissolution of the Eocene dolostones argue against the postulation by Ehrenberg, et al. (2012).

VI. Conclusion

The main conclusions that can be derived from this petrographic and petrophysical study of the Eocene Avanah dolostones in northeastern Iraq include:

1. Deposition of the carbonate, meteoric water incursion, and dolomitization are attributed to cycles of 4th order relative sea-level change, which controlled the degree of water circulation restriction in the inner ramp.
2. The lack of evaporites in the succession suggests that dolomitization has occurred by seepage reflux of mesohaline/penesaline brines evolved by evaporation of semi-restriction lagoon water body during a substantial fall in the RSL.
3. Before dolomitization during each sea-level cycle, the carbonate sediments were subjected to: (i) seafloor cementation by scalenohedral calcite and (ii) dissolution of aragonite allochems by the incursion of undersaturated meteoric water and cementation by equant calcite.
4. The dolostones were subsequently subjected to substantial dissolution by upward flow of aggressive hypogenic, basinal fluids. More extensive dissolution (i.e., greater extent of porosity and permeability enhancement) and cementation by intercrystalline occurred in the flank well, denoting the role of oil emplacement in retarding/inhibiting diagenetic alterations. The flow of basinal fluids is supported by the presence of small amounts of anhydrite and K-feldspar cements.

VII. Acknowledgment

The author would like to express gratitude to the Ministry of Natural Resources and Kar Company for their support and for granting permission to use the provided data. Appreciation is also extended to the Earth Sciences and Petroleum Department, Salahaddin University-Erbil, for their continuous support. Special appreciation is given to Dr. Mohammad Alsuwaidi from the Earth Science Department at Khalifa University for his valuable assistance and guidance throughout this research. The author also wishes to thank the anonymous reviewers and Dr. Salah I. Yahya, Editor of ARO, for their constructive feedback and valuable suggestions, which significantly enhanced the quality of this manuscript.

References

Adams, J.E., and Rhodes, M.L., 1960. Dolomitization by seepage refluxion. *AAPG Bulletin*, 44, pp.1912-1920.

Al-Ameri, T.K., 2010. Palynostratigraphy and the assessment of gas and oil generation and accumulations in the Lower Paleozoic, Western Iraq. *Arabian Journal of Geosciences*, 3, pp.155-179.

Alavi, M., 2004. Regional stratigraphy of the Zagros fold-thrust belt of Iran and its proforeland evolution. *American Journal of Science*, 304, pp.1-20.

Al-Helal, A.B., Whitaker, F.F., and Xiao, Y., 2012. Reactive transport modeling of brine reflux: Dolomitization, anhydrite precipitation, and porosity evolution. *Journal of Sedimentary Research*, 82, pp.196-215.

Al-Zubaidi, A., and Al-Badrani, O., 2019. Paleoclimatology evidence of eocene from jaddala formation in northwestern Iraq. In: *Patterns and Mechanisms of Climate, Paleoclimate and Paleoenvironmental Changes from Low-Latitude Regions: Proceedings of the 1st Springer Conference of the Arabian Journal of Geosciences (CAJG-1),* Tunisia 2018, pp.33-35.

Ameen, B.M., 2009. Lithological indicators for the Oligocene unconformity, NE Iraq. *Iraqi Bulletin of Geology and Mining*, 5, pp.25-34.

Aqrawi, A.A.M., Mahdi, T.A., Sherwani, G.H., and Horbury, A.D., 2010. Characterization of the mid-cretaceous mishrif reservoir of the southern Mesopotamian basin, Iraq. In: *American Association of Petroleum Geologists Conference and Exhibition*. Vol. 7. pp.7-10.

Barth, T., 1991. Organic acids and inorganic ions in waters from petroleum reservoirs, Norwegian continental shelf: A multivariate statistical analysis and comparison with American reservoir formation waters. *Applied Geochemistry*, 6, pp.1-15.

Berberian, M., 1995. Master "blind" thrust faults hidden under the Zagros folds: Active basement tectonics and surface morphotectonics. *Tectonophysics*, 241, pp.193-224.

Boles, J.R., 1992. Book review: Prediction of reservoir quality through geochemical modeling. ID Meshri and PJ Ortoleva (Editors). Memoir 49, Amer. Assoc. Petrol. Geol., Tulsa, OK, 1990, ISBN 0-89181-327-6, 175 pp., US46. 00 (AAPG members), US69. 00 (non-members). *Journal of Geochemical Exploration*, 43, pp.293-294.

Braithwaite, C.J.R., 1991. Dolomites, a review of origins, geometry and textures. *Earth and Environmental Science Transactions of The Royal Society of Edinburgh*, 82, pp.99-112.

Carballo, J., Land, L.S., and Miser, D.E., 1987. Holocene dolomitization of supratidal sediments by active tidal pumping, Sugarloaf Key, Florida. *Journal of Sedimentary Research*, 57, pp.153-165.

Carothers, W.W., and Kharaka, Y.K., 1978. Aliphatic acid anions in oil-field waters-implications for origin of natural gas. *AAPG Bulletin*, 62, pp.2441-2453.

Carothers, W.W., and Kharaka, Y.K., 1980. Stable carbon isotopes of HCO3− in oil-field waters-implications for the origin of CO_2. *Geochimica et Cosmochimica Acta*, 44, pp.323-332.

Chen, L., Zhang, H., Cai, Z., Hao, F., Xue, Y., and Zhao, W., 2022. Petrographic, mineralogical and geochemical constraints on the fluid origin and multistage karstification of the Middle-Lower Ordovician carbonate reservoir, NW Tarim Basin, China. *Journal of Petroleum Science and Engineering*, 208, p.109561.

Choquette, P.W. and Pray, L.C., 1970. Geologic nomenclature and classification of porosity in sedimentary carbonates. *AAPG Bulletin*, 54, pp.207-250.

Cooles, G.P., Mackenzie, A.S., and Parkes, R.J., 1987. Non-hydrocarbons of significance in petroleum exploration: Volatile fatty acids and non-hydrocarbon gases. *Mineralogical Magazine*, 51, pp.483-493.

Cosmo, R.D.P., Rinaldi, R., Pereira, F.D.A.R., Soares, E.J., and Martins, A.L., 2023. CO_2 degassing in CaCO3 precipitation in the presence of oil: Implications, modeling, numerical simulation, validation, prototype development, and experimental results. *Geoenergy Science and Engineering*, 228, p.211885.

Cox, P.A., Wood, R.A., Dickson, J.A.D., Al Rougha, H.B., Shebl, H., and Corbett, P.W.M., 2010. Dynamics of cementation in response to oil charge: Evidence from a Cretaceous carbonate field, UAE. *Sedimentary Geology*, 228, pp.246-254.

Crossey, L.J., 1991. Thermal degradation of aqueous oxalate species. *Geochimica et Cosmochimica Acta*, 55, pp.1515-1527.

Dias, R.F., 2000. *Stable Carbon-Isotope Geochemistry of Low-Molecular Weight Organic Acids in oil-Associated Waters*. The Pennsylvania State University, United States.

Dunham, R.J., 1962. Classification of carbonate rocks according to depositional texture. *AAPG Memoir,* 1, pp.108-121.

Eglinton, T.I., Curtis, C.D., and Rowland, S.J., 1987. Generation of water-soluble organic acids from kerogen during hydrous pyrolysis: Implications for porosity development. *Mineralogical Magazine*, 51, pp.495-503.

Ehrenberg, S.N., Eberli, G.P., Keramati, M., and Moallemi, S.A., 2006. Porosity-permeability relationships in interlayered limestone-dolostone reservoirs. *AAPG Bulletin*, 90, pp.91-114.

Ehrenberg, S.N., Walderhaug, O., and Bjørlykke, K., 2012. Carbonate porosity creation by mesogenetic dissolution: Reality or illusion? *AAPG Bulletin*, 96, pp.217-233.

Franks, S.G., Dias, R.F., Freeman, K.H., Boles, J.R., Holba, A., Fincannon, A.L., and Jordan, E.D., 2001. Carbon isotopic composition of organic acids in oil field waters, San Joaquin Basin, California, USA. *Geochimica et Cosmochimica Acta*, 65, pp.1301-1310.

Giles, M.R., and Marshall, J.D., 1986. Constraints on the development of secondary porosity in the subsurface: Re-evaluation of processes. *Marine and Petroleum Geology*, 3, pp.243-255.

Hanor, J.S., 1994. Origin of saline fluids in sedimentary basins. *Geological Society, London, Special Publications*, 78, pp.151-174.

Hearn, P.P. Jr., and Sutter, J.F., 1985. Authigenic potassium feldspar in Cambrian carbonates: Evidence of Alleghanian brine migration. *Science*, 228, pp.1529-1531.

Heasley, E.C., Worden, R.H., and Hendry, J.P., 2000. Cement distribution in a carbonate reservoir: Recognition of a palaeo oil-water contact and its relationship to reservoir quality in the Humbly Grove field, onshore, UK. *Marine and Petroleum Geology*, 17, pp.639-654.

Jassim, S.Z., and Goff, J.C. editors., 2006. *Geology of Iraq. DOLIN, sro*. Distributed by Geological Society of London, London.

Jia, C., Alkaabi, S., Sepehrnoori, K., Fan, D., and Yao, J., 2023. Numerical modeling and studies of the acid stimulation process in dolomite carbonate rocks. *SPE Journal*, 28, pp.2165-2185.

Jones, D.L., Dennis, P.G., Owen, A.G., and Van Hees, P.A.W., 2003. Organic acid behavior in soils-misconceptions and knowledge gaps. *Plant and Soil*, 248, pp.31-41.

Jones, G.D., and Xiao, Y., 2005. Dolomitization, anhydrite cementation, and porosity evolution in a reflux system: Insights from reactive transport models. *AAPG Bulletin*, 89, pp.577-601.

Joseph, I.A., Ajala, E.O., Ahmed, E.L.A., and Ajala, M.A., 2022. Optimization and kinetics studies of the dissolution of dolomite in sulphuric acid (H_2SO_4) via Box-Behnken experimental design. *Southern Journal of Sciences,* 30, pp.69-81.

Katz, D.A., Eberli, G.P., Swart, P.K., and Smith, L.B., 2006. Tectonic-hydrothermal brecciation associated with calcite precipitation and permeability destruction in Mississippian carbonate reservoirs, Montana and Wyoming. *AAPG Bulletin*, 90, pp.1803-1841.

Kawamura, K., Tannenbaum, E., Huizinga, B.J., and Kaplan, I.R., 1986. Volatile organic acids generated from kerogen during laboratory heating. *Geochemical Journal*, 20, pp.51-59.

Kerans, C., and Tinker, S.W., 1997. *Sequence Stratigraphy and Characterization of Carbonate Reservoirs.* Tulsa: SEPM. 40, p.130.

Khanaqa, P.A., 2011. Interpretation of new facies in the Pila Spi formation (middle-late eocene), in Sulaimaniyah, NE Iraq. *Iraqi Bulletin of Geology and Mining*, 7, pp.33-45.

Klimchouk, A.B., 2000. Lithologic and structural controls of dissolutional cave development. In: Dreybrodt, W., Ford, D.C., Palmer, A.N., and Klimchouk, A.B. (eds), *Speleogenesis, Evolution of Karst Aquifers*, National Speleological Society, Huntsville, AL, p.54-64.

Klimchouk, A.B., 2017. Types and settings of hypogene karst. Chapter In: *Hypogene Karst Regions and Caves of the World*. Springer, Berlin, p.1-39.

Koeshidayatullah, A., Corlett, H., Stacey, J., Swart, P.K., Boyce, A., Robertson, H., Whitaker, F., and Hollis, C., 2020. Evaluating new fault-controlled hydrothermal dolomitization models: Insights from the Cambrian Dolomite, Western Canadian Sedimentary Basin. *Sedimentology*, 67, pp.2945-2973.

Laya, J.C., Teoh, C.P., Whitaker, F., Manche, C., Kaczmarek, S., Tucker, M., Gabellone, T., and Hasiuk, F., 2021. Dolomitization of a Miocene-Pliocene progradational carbonate platform by mesohaline brines: Re-examination of the reflux model on Bonaire Island. *Marine and Petroleum Geology*, 126, p.104895.

Le Garzic, E., Vergés, J., Sapin, F., Saura, E., Meresse, F., and Ringenbach, J.C., 2019. Evolution of the NW Zagros Fold-and-Thrust Belt in Kurdistan Region of Iraq from balanced and restored crustal-scale sections and forward modeling. *Journal of Structural Geology*, 124, pp.51-69.

Leary, D.A., and Vogt, J.N., 1987. *Diagenesis of Permian (guadalupian) San Andres formation, Central Basin Platform, West Texas*. AAPG (American Association of Petroleum Geologists) Bull, United States, p.71(CONF-870606-).

Li, Q., Wang, L., Fu, Y., Lin, D., Hou, M., Li, X., Hu, D., and Wang, Z., 2023. Transformation of soil organic matter subjected to environmental disturbance and preservation of organic matter bound to soil minerals: A review. *Journal of Soils and Sediments*, 23, pp.1485-1500.

Lucia, F.J., 2004. Origin and petrophysics of dolostone pore space. *Geological Society, London, Special Publications*, 235, pp.141-155.

Lucia, F.J., and Major, R.P., 1994. *Porosity Evolution through Hypersaline Reflux Dolomitization*. A volume in honour of Dolomieu, Dolomites, pp.325-341.

Lundegard, P.D., and Land, L.S., 1986. Carbon dioxideandorganic acids: Their role in porosity enhancement and cementation, Pa leogene of the Texas Gulf Coast. In: Gautier, D.L., editor. *Roles of Organic Matter in Sediment Diagenesis*. SEPM Special Publication, Tulsa, pp.129-146.

Lundegard, P.D., Land, L.S., and Galloway, W.E., 1984. Problem of secondary porosity: Frio formation (oligocene), texas gulf coast. *Geology*, 12, pp.399-402.

MacGowan, D.B., and Surdam, R.C., 1990. Carboxylic acid anions in formation waters, San Joaquin Basin and Louisiana Gulf Coast, USA-implications for clastic diagenesis. *Applied Geochemistry*, 5, pp.687-701.

Machel, H.G., 2004. Concepts and models of dolomitization: A critical reappraisal. *Geological Society London Special Publications*, 235, pp.7-63.

Machel, H.G., and Mountjoy, E.W., 1986. Chemistry and environments of dolomitization-a reappraisal. *Earth-Science Reviews*, 23, pp.175-222.

Mahmood, B.S., Khoshnaw, F.A., Abdalqadir, M.O., and Gomari, S.R., 2023. Natural fracture characterization and *in situ* stress orientation analysis using fullbore formation micro imager (FMI): A case study on the X oil field, Kurdistan Region, Iraq. *Arabian Journal of Geosciences*, 16, p.113.

Mansurbeg, H., Alsuwaidi, M., Morad, D., Morad, S., Tiepolo, M., Shahrokhi, S., Al-Aasm, I.S., and Koyi, H., 2024. Disconformity-controlled hydrothermal dolomitization and cementation during basin evolution: Upper Triassic carbonates, UAE. *Geology*, 52, pp.486-491.

Mansurbeg, H., Morad, D., Othman, R., Morad, S., Ceriani, A., Al-Aasm, I., Kolo, K., Spirov, P., Proust, J.N., Preat, A., and Koyi, H., 2016. Hydrothermal dolomitization of the Bekhme formation (Upper Cretaceous), Zagros Basin, Kurdistan Region of Iraq: Record of oil migration and degradation. *Sedimentary Geology*, 341, pp.147-162.

Martín-Martín, J.D., Travé, A., Gomez-Rivas, E., Salas, R., Sizun, J.P., Vergés, J., Corbella, M., Stafford, S., and Alfonso, P., 2015. Fault-controlled and stratabound dolostones in the Late Aptian-earliest Albian Benassal Formation (Maestrat Basin, E Spain): Petrology and geochemistry constrains. *Marine and Petroleum Geology*, 65, pp.83-102.

Mazzullo, S.J., 2000. Organogenic dolomitization in peritidal to deep-sea sediments. *Journal of Sedimentary Research*, 70, pp.10-23.

Merino, E., and Canals i Sabaté, À., 2011. Self-accelerating dolomite-for-calcite replacement: Self-organized dynamics of burial dolomitization and associated mineralization. *American Journal of Science*, 311, pp.573-607.

Morad, D., Nader, F.H., Gasparrini, M., Morad, S., Rossi, C., Marchionda, E., Al Darmaki, F., Martines, M., and Hellevang, H., 2018. Comparison of the diagenetic and reservoir quality evolution between the anticline crest and flank of an Upper Jurassic carbonate gas reservoir, Abu Dhabi, United Arab Emirates. *Sedimentary Geology*, 367, pp.96-113.

Morad, D., Nader, F.H., Morad, S., Rossi, C., Gasparrini, M., Alsuwaidi, M., Al Darmaki, F., and Hellevang, H., 2019. Limited thermochemical sulfate reduction in hot, anhydritic, sour gas carbonate reservoirs: The Upper Jurassic Arab Formation,

United Arab Emirates. *Marine and Petroleum Geology*, 106, pp.30-41.

Morad, S., Al Suwaidi, M., Mansurbeg, H., Morad, D., Ceriani, A., Paganoni, M., and Al-Aasm, I., 2019. Diagenesis of a limestone reservoir (Lower Cretaceous), Abu Dhabi, United Arab Emirates: Comparison between the anticline crest and flanks. *Sedimentary Geology*, 380, pp.127-142.

Morad, S., Al-Aasm, I.S., Nader, F.H., Ceriani, A., Gasparrini, M., and Mansurbeg, H., 2012. Impact of diagenesis on the spatial and temporal distribution of reservoir quality in the Jurassic Arab D and C members, offshore Abu Dhabi oilfield, United Arab Emirates. *GeoArabia,* 17, pp.17-56.

Morad, S., Farooq, U., Mansurbeg, H., Alsuwaidi, M., Morad, D., Al-Aasm, I.S., Shahrokhi, S., Hozayen, M., and Koyi, H., 2023. Variations in extent, distribution and impact of dolomitization on reservoir quality of Upper Cretaceous foreland-basin carbonates, Abu Dhabi, United Arab Emirates. *Marine and Petroleum Geology*, 155, p.106357.

Morrow, D.W., 1982. Diagenesis 1. Dolomite-Part 1: The chemistry of dolomitization and dolomite precipitation. *Geoscience Canada,* 9, pp.5-13.

Omidpour, A., Mahboubi, A., Moussavi-Harami, R., and Rahimpour-Bonab, H., 2022. Effects of dolomitization on porosity-Permeability distribution in depositional sequences and its effects on reservoir quality, a case from Asmari Formation, SW Iran. *Journal of Petroleum Science and Engineering*, 208, p.109348.

Paganoni, M., Al Harthi, A., Morad, D., Morad, S., Ceriani, A., Mansurbeg, H., Al Suwaidi, A., Al-Aasm, I.S., Ehrenberg, S.N., and Sirat, M., 2016. Impact of stylolitization on diagenesis of a Lower Cretaceous carbonate reservoir from a giant oilfield, Abu Dhabi, United Arab Emirates. *Sedimentary Geology*, 335, pp.70-92.

Palmer, A.N., 2013. Sulfuric acid caves: Morphology and evolution. In: Shroder, J.F., editor. *Treatise on Geomorphology*. Vol. 6. Academic Press, San Diego, pp.241-257.

Palmer, D.A., and Drummond, S.E., 1986. Thermal decarboxylation of acetate. Part I. The kinetics and mechanism of reaction in aqueous solution. *Geochimica et Cosmochimica Acta*, 50, pp.813-823.

Qing, H., Bosence, D.W., and Rose, E.P., 2001. Dolomitization by penesaline sea water in Early Jurassic peritidal platform carbonates, Gibraltar, western Mediterranean. *Sedimentology*, 48, pp.153-163.

Rameil, N., 2008. Early diagenetic dolomitization and dedolomitization of Late Jurassic and earliest Cretaceous platform carbonates: A case study from the Jura Mountains (NW Switzerland, E France). *Sedimentary Geology*, 212, pp.70-85.

Roberts, J.A., Kenward, P.A., Fowle, D.A., Goldstein, R.H., González, L.A., and Moore, D.S., 2013. Surface chemistry allows for abiotic precipitation of dolomite at low temperature. *Proceedings of the National Academy of Sciences*, 110, pp.14540-14545.

Schulz-Rojahn, J., Ryan-Grigor, S., and Anderson, A., 1998. Structural controls on seismic-scale carbonate cementation in hydrocarbon-bearing jurassic fluvial and marine sandstones from Australia: A comparison. In: *Carbonate Cementation in Sandstones: Distribution Patterns and Geochemical Evolution*. Wiley, United States, pp.327-362.

Sharland, P.R., Casey, D.M., Davies, R.B., Simmons, M.D., and Sutcliffe, O.E., 2004. Arabian plate sequence stratigraphy-revisions to SP2. *GeoArabia*, 9, pp.199-214.

Simmons, M.D., Sharland, P.R., Casey, D.M., Davies, R.B., and Sutcliffe, O.E., 2007. Arabian Plate sequence stratigraphy: Potential implications for global chronostratigraphy. *GeoArabia*, 12, pp.101-130.

Sissakian, V.K., and Al-Jiburi, B.S., 2014. Stratigraphy of the high folded zone. *Iraqi Bulletin of Geology and Mining,* 6, pp.73-161.

Smith, R.A., Ditmire, T., and Tisch, J.W.G., 1998. Characterization of a cryogenically cooled high-pressure gas jet for laser/cluster interaction experiments. *Review of Scientific Instruments*, 69, pp.3798-3804.

Spötl, C., Kunk, M.J., Ramseyer, K., and Longstaffe, F.J., 1998. Authigenic potassium feldspar: A tracer for the timing of palaeofluid flow in carbonate rocks, Northern Calcareous Alps, Austria. *Geological Society, London, Special Publications*, 144, pp.107-128.

Sun, S.Q., 1995. Dolomite reservoirs: Porosity evolution and reservoir characteristics. *AAPG Bulletin,* 79, pp.186-204.

Surdam, R.C., Boese, S.W., and Crossey, L.J., 1984. The chemistry of secondary porosity. *Memoir of the American Association of Petroleum Geologists*, 37, pp.127-149.

Tavakoli, V., and Barfizadeh, H., 2024. The role of plate movements on reservoir development of the Iranian carbonate formations: A review of the interplay between tectonics, paleoclimate, and diagenesis. *Results in Earth Sciences*, 2, p.100037.

Turner, L.K., and Collins, F.G., 2013. Carbon dioxide equivalent (CO2-e) emissions: A comparison between geopolymer and OPC cement concrete. *Construction and Building Materials*, 43, pp.125-130.

Wahlman, G.P., 2010. Reflux dolomite crystal size variation in cyclic inner ramp reservoir facies, Bromide Formation (Ordovician), Arkoma Basin, southeastern Oklahoma. *The Sedimentary Record*, 8, pp.4-9.

Warren, J., 2000. Dolomite: Occurrence, evolution and economically important associations. *Earth-Science Reviews*, 52, pp.1-81.

Wierzbicki, R., Dravis, J.J., Al-Aasm, I., and Harland, N., 2006. Burial dolomitization and dissolution of upper Jurassic Abenaki platform carbonates, deep Panuke reservoir, Nova Scotia, Canada. *AAPG Bulletin*, 90, pp.1843-1861.